XVIII Convegno Nazionale IGF
Cetraro (CS), 31 Maggio – 1 Giugno 2006

DYNAMIC FAILURE, BRANCHING AND FRAGMENTATION USING COHESIVE ZONE MODELING

Glaucio H. Paulino[a], Zhengyu Zhang[b], and Waldemar Celes[c]

[a] *Department of Civil and Environmental Engineering, University of Illinois at Urbana-Champaign, Newmark Laboratory, 205 North Mathews Avenue, Urbana, IL 61801-2397, USA. e-mail:paulino@uiuc.edu*

[b] *Department of Civil and Environmental Engineering, University of Illinois at Urbana-Champaign, Newmark Laboratory, 205 North Mathews Avenue, Urbana, IL 61801-2397, USA. e-mail:zzhang3@uiuc.edu*

[c] *Tecgraf/PUC-Rio Computer Science Department, Pontifical Catholic University of Rio de Janeiro, Rua Marquês de São Vicente 225, Rio de Janeiro, RJ, 22450-900, Brazil. e-mail:celes@inf.puc-rio.br*

ABSTRACT

This paper presents a computational framework appropriate for dynamic crack branching and fragmentation processes investigation. The finite element method incorporates special interface elements based on a cohesive zone model (CZM) to characterize the fracture process. A novel topology-based data structure is employed to facilitate fast and robust manipulation of evolving mesh information when extrinsic cohesive elements are inserted adaptively. To illustrate the application of the method, a set of "quasi-steady-state" crack propagation experiments exhibiting micro-branching phenomena in Polymethylmethacrylate (PMMA) are numerically simulated. The simulation results compare reasonably well with experimental observations both globally and locally, and demonstrate certain advantageous features of the extrinsic CZM with respect to the intrinsic CZM.

1 INTRODUCTION

Dynamic fracture instability in brittle materials has been a field of much interest and research during the past decades [1]. Experiments have been performed on various amorphous brittle materials to investigate dynamic fracture behavior; for instance, Homalite-100 [6, 7, 8, 9], PMMA [11, 10], Solithane-113 and polycarbonate [10]. Two phenomena remained the focus of interest among these observations: first, crack surface roughens as crack speeds up, as the "mirror-mist-hackle" stages described in [8]; second, the onset of instability occurs at a speed well below the theoretical limiting speed predicted by classical linear elastodynamics. Although crack instability at high speed is predicted by the conventional linear elastodynamic theory, these experimental observations reveal significant deviation of fracture behavior in the brittle material from those conditions suggested by the linear theory.

This work investigates dynamic crack microbranching processes by incorporating a cohesive zone model (CZM) in the finite element method to characterize the fracture process. One major challenge in simulating branching and fragmentation phenomena is how to allow multiple cracks to form "freely" in a finite discretization. Among the set of numerical schemes in the literature, the CZM has the advantage of allowing multiple crack formation. Between the two classes of CZMs, *i.e.*, "*intrinsic*" and "*extrinsic*" models, the latter is adopted in the study as this approach avoids a number of disadvantages of the former, including the so-called "artificial compliance", which may result in significant reduction of stiffness of the modelled specimen. The extrinsic CZM employed in the finite element scheme is characterized by a finite cohesive strength at onset of material weakening and work to fracture. The implementation of the extrinsic CZM approach is facilitated by a novel data structure that allows convenient and robust access to adjacency information as well as adaptive insertion of cohesive elements during the course of the simulation [2, 3].

2 INTRINSIC VERSUS EXTRINSIC COHESIVE ZONE MODEL

The concept of "cohesive failure" is illustrated in Figure 1 (a) for tensile (mode I) case. At the immediate vicinity of crack tip, the material cannot sustain infinitely high stress, and material softens, which results, for example, from void growth and microcrack formation. This status is simulated with the traction-separation relationship law inside the *cohesive zone*, which is along the plane of potential crack propagation. Within the extent of the cohesive zone, the material points which were identical when the material was intact, separate to a distance Δ due to the influence of the stress state at the crack tip vicinity. The cohesive zone surface sustains a distribution of tractions T which are function of the displacement jump across the surface Δ, and the relationship between the traction T and separation Δ is defined as the constitutive law for the cohesive zone surface.

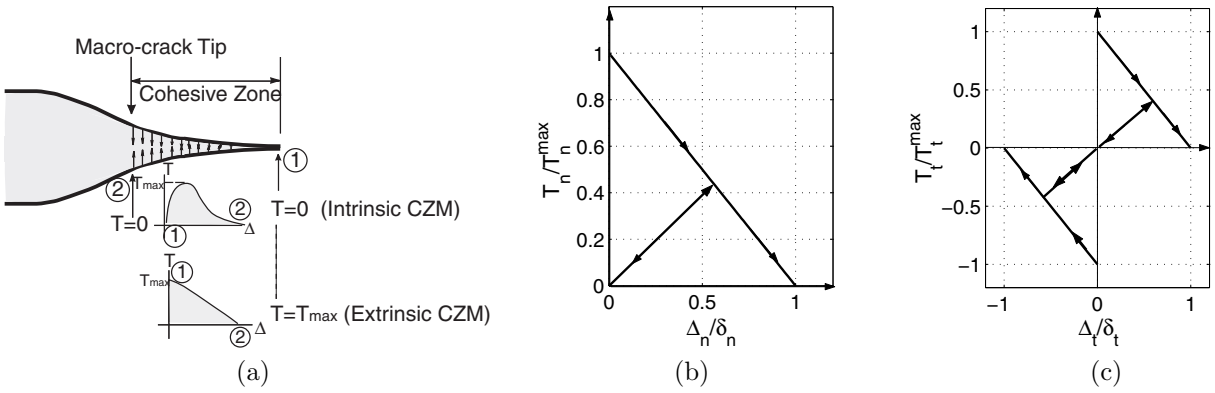

Figure 1: Cohesive zone concept and extrinsic CZM; (a) CZM considers material softening and separation using distributed cohesive tractions along a cohesive surface at the crack tip vicinity. Circled numbers ① and ② denote the corresponding positions on the cohesive zone and cohesive law curves where material begins to soften (①) and where material completely loses fracture resistance capacity (②); (b) initially-rigid extrinsic cohesive zone model [5] in pure tension; (c) initially-rigid extrinsic cohesive zone model [5] in pure shear.

CZMs can be categorized into two major groups: intrinsic CZMs and extrinsic CZMs. The main distinction between intrinsic and extrinsic CZMs is the presence of the initial elastic curve, as shown in Figure 1 (a). Intrinsic CZMs assume that, *e.g.* in pure tension case, traction T_n first increases with increasing interfacial separation Δ_n, reaches a maximum value T_n^{max}, then decreases and finally vanishes at a characteristic separation value δ_n, where complete decohesion is assumed to occur. On the other hand, extrinsic CZMs assume that separation only occurs when the interfacial traction reaches the finite strength T_n^{max}, and once the separation occurs, the interfacial cohesion force monotonically decreases as separation increases.

In the present study, the model by Ortiz and Pandolfi [5] is employed, as shown in Figure 1 (b) and (c). This model eliminates the artificial softening effect due to elastic deformation of cohesive interface present in intrinsic models such as Xu and Needleman's [14]. In the implementation stage, the cohesive elements are adaptively inserted into the mesh, *i.e.* the initial topology of the mesh does not contain any cohesive elements. When a certain fracture criterion is met, a cohesive element is inserted at the proper location of the mesh, which allows the crack to propagate.

This model defines *effective traction* T_{eff} and *effective displacement* Δ_{eff} as

$$T_{\text{eff}} = \sqrt{T_{\text{n}}^2 + \eta^{-2} T_{\text{t}}^2}, \qquad \Delta_{\text{eff}} = \sqrt{\Delta_{\text{n}}^2 + \eta^2 \Delta_{\text{t}}^2} \qquad \text{for } T_{\text{n}} \geq 0, \tag{1a}$$

$$T_{\text{eff}} = \left(|T_{\text{t}}|\right)/\eta, \qquad \Delta_{\text{eff}} = \eta \left(|\Delta_{\text{t}}|\right) \qquad \text{for } T_{\text{n}} < 0 \tag{1b}$$

where T_n and T_t are the cohesive tractions in normal and tangential direction, respectively; η is the shear stress factor, which represents the mode mixity effect. When the fracture initiation condition $T_{\text{eff}} \geq T_{\text{n}}^{\max}$ is met, a new surface is introduced into the mesh by doubling nodes and creating interface cohesive elements.

The cohesive force that resists the opening and sliding of the new surface is assumed to weaken irreversibly with increasing crack opening. Irreversibility is retained by keeping track of the maximum displacement in the simulation history and by using it as the indicator for loading or unloading.

Under loading condition, when the current effective opening displacement Δ_{eff} is larger than that in the history $\Delta_{\text{eff}_{(\max)}}$, the cohesive traction ramps down linearly as displacement jump increases, and reduces to zero as opening reaches critical opening displacement $\Delta_n = \delta_n$. The decohesion is complete at this point and cohesive force vanishes thereafter. Thus

$$T_{\text{n}} = T_{\text{n}}^{\max}\left(1 - \frac{\Delta_{\text{eff}}}{\delta_{\text{n}}}\right)\frac{\Delta_{\text{n}}}{\Delta_{\text{eff}}}; \qquad T_{\text{t}} = \eta T_{\text{n}}^{\max}\left(1 - \frac{\Delta_{\text{eff}}}{\delta_{\text{n}}}\right)\frac{\Delta_{\text{t}}}{\Delta_{\text{eff}}} \tag{2}$$

If unloading occurs, the crack begins to close, and the traction obeys the linear unloading relation, assuming unloading towards the origin:

$$T_{\text{n}} = T_{\text{n}}^{\max}\left(1 - \frac{\Delta_{\text{eff}_{\max}}}{\delta_{\text{n}}}\right)\frac{\Delta_{\text{n}}}{\Delta_{\text{eff}_{(\max)}}}; \qquad T_{\text{t}} = \eta T_{n}^{\max}\left(1 - \frac{\Delta_{\text{eff}_{\max}}}{\delta_{\text{n}}}\right)\frac{\Delta_{\text{t}}}{\Delta_{\text{eff}_{(\max)}}} \tag{3}$$

as shown in Figure 1 (b) and (c). If the crack reopens, the reloading path follows the unloading path in the reverse direction until $\Delta_{\text{eff}_{(\max)}}$ and then follows the original ramp-down relation (2).

3 FINITE ELEMENT SCHEME INCORPORATING COHESIVE ELEMENTS

To incorporate a CZM into the numerical scheme for dynamic fracture simulation, the *cohesive element* is developed and implemented as part of the finite element scheme, which follows a cohesive *traction-separation* relationship. In contrast, the conventional volumetric finite element, which is now called "*bulk* element", follows conventional *stress-strain* relationships (continuum description).

To model fracture initiation and propagation, cohesive elements are inserted "on-the-fly" to the existing mesh, positioned along the predicted crack path, and attached to the bulk elements. Once inserted, the cohesive elements produce cohesive traction that resists opening, depending on the interface separation by the cohesive law. When interface opening exceeds critical value, the element loses all capacity against separation and crack advances. The constitutive law of cohesive elements is inherently embedded in the finite element model, so that the presence of cohesive elements allows spontaneous crack propagation, and thus it is very promising in the investigation of bifurcation and/or of impact dynamic loading, where multiple crack paths are possible. The difficulty of employing extrinsic cohesive model in finite element method, however, resides in the extensive updating of mesh and topological information as crack advances, which is discussed in Section 4.

The FEM formulation incorporating cohesive elements is derived from the principle of virtual work, and discretized using the explicit central difference time stepping scheme to update displacements $\mathbf{u}$, accelerations $\ddot{\mathbf{u}}$ and velocities $\dot{\mathbf{u}}$ as follows:

$$\mathbf{u}_{n+1} = \mathbf{u}_n + \Delta t\dot{\mathbf{u}}_n + \frac{1}{2}(\Delta t)^2\ddot{\mathbf{u}}_n \tag{4}$$

$$\ddot{\mathbf{u}}_{n+1} = \mathbf{M}^{-1}(\mathbf{F} - \mathbf{R}_{int_{(n+1)}} + \mathbf{R}_{coh_{(n+1)}}) \tag{5}$$

$$\dot{\mathbf{u}}_{n+1} = \dot{\mathbf{u}}_n + \frac{\Delta t}{2}(\ddot{\mathbf{u}}_n + \ddot{\mathbf{u}}_{n+1}) \tag{6}$$

where Δt denotes the time step, $\mathbf{M}$ is the lumped mass matrix, $\mathbf{F}$ is the external force vector, $\mathbf{R}_{int}$ and $\mathbf{R}_{coh}$ are the global internal and cohesive force vectors, which are obtained from the contribution of *bulk* and *cohesive* elements, respectively. Large deformation formulation is employed [15].

4 FRAMEWORK USING THE TOPOLOGICAL DATA STRUCTURE (TOPS)

Topological Framework for Cohesive Element Insertion. Extrinsic CZMs require modifications of the mesh during the course of the simulation for the adaptive insertion of new cohesive elements along bulk element interfaces. In order to efficiently handle such modifications, the mesh has to be described by means of a

topological data structure, thus acquiring efficient access to the topological adjacency relationships among the defined topological entities. In this work, the adjacency-based topological data structure (TopS) presented in our previous work [3] is used. In this data structure (TopS), only nodes and elements are explicitly stored. All other defined topological entities are implicit, and their representations are retrieved, as required, "on-the-fly". As a consequence, the memory space required to store the mesh is reduced, thus being appropriate for large models.

Besides *node* and *element*, the data structure defines (and implicitly represents) three topological entities: *facet*, *edge*, and *vertex*. The topological data structure provides support for the insertion of cohesive elements along any facet that represents the interface between two bulk elements. The insertion of a cohesive element may require the duplication of nodes, thus changing the connectivity of neighboring elements. Whether a node has to be duplicated or not depends on the topological classification of the fractured facet. All mesh modifications due to the insertion of a new cohesive element are based on local topological operations, thus being performed very efficiently: the time needed to insert a new cohesive element is proportional to the number of topological entities adjacent to the fractured facet [3].

Criteria to Insert Cohesive Elements The topological data structure (TopS) is a modular computational layer which can be interfaced with any analysis code. In the present work, the insertion of new cohesive elements along the interfaces between bulk elements is performed by the following procedure at chosen time intervals:

- *Calculate the stress along each facet:* for each facet between two bulk elements in the entire domain, compute the traction components along the outer normal of the facet, and the effective stress T_{eff}.
- *Flag fractured facets:* when criterion $T_{\text{eff}} \geq T_n^{max}$ is satisfied, the facet is flagged to be the site of cohesive element insertion.
- *Insert cohesive elements:* call the topological data structure (TopS) functions to insert new cohesive elements along fractured facets, updating the attributes of elements and nodes.

Topological Operations to Insert Cohesive Elements Once identified the facet along which a new cohesive element has to be inserted, the data structure performs a set of topological operations in order to update the mesh. Considering a triangular mesh, the set of operations is given by:

- *Classify the facet against the mesh boundary:* for each bounding vertex of the edge associated to the fractured facet, the data structure checks whether it lays on the mesh boundary. This checking is done by retrieving all adjacent facets around the vertex and verifying if any of them represents the interface between a bulk element and the external boundary or between a bulk element and an existing cohesive element.
- *Duplicate the mid-side nodes:* for quadratic (or higher order) elements, duplicate the mid-side nodes along the edge associated to the fractured facet.
- *Duplicate the corner nodes, if necessary:* for each vertex on the boundary, duplicate the associated element-corner node.
- *Update the element incidences:* for each duplicated node, update the incidence of adjacent elements. The data structure identifies which elements must have their incidence updated.
- *Insert a new cohesive element in the model:* insert a new cohesive element with incidence given by the new set of nodes along the fractured facet.

5 NUMERICAL EXAMPLE

Sharon and his co-workers [12, 11, 13] investigated "quasi-steady-state crack propagation", i.e. the crack runs at a relatively constant speed throughout the strip. The study focuses on characterization of the relationship

between microcrack pattern, crack surface characteristics and crack speed. Due to the large dimension of original specimen, the numerical investigation uses a geometry of reduced dimension in comparison with the original experiment, however, most of the features of the experiment are well reproduced.

5.1 Problem Description

Figure 2 (a) shows the geometry and boundary conditions used in the study. The strip is initially stretched uniformly by imposing an initial displacement field

$$u(x, y; t = 0) = 0, \quad v(x, y; t = 0) = \varepsilon y \tag{7}$$

which results in a uniform strain field at the initial time. The upper and lower surfaces are held fixed and a small crack length a is introduced at the left edge at time $t = 0$. The material used is Polymethylmethacrylate (PMMA) [14], and its properties are given in Table 1. In the numerical simulations G_{IIc} is assumed to be equal to G_{Ic} ($G_{\mathrm{IIc}} = G_{\mathrm{Ic}}$).

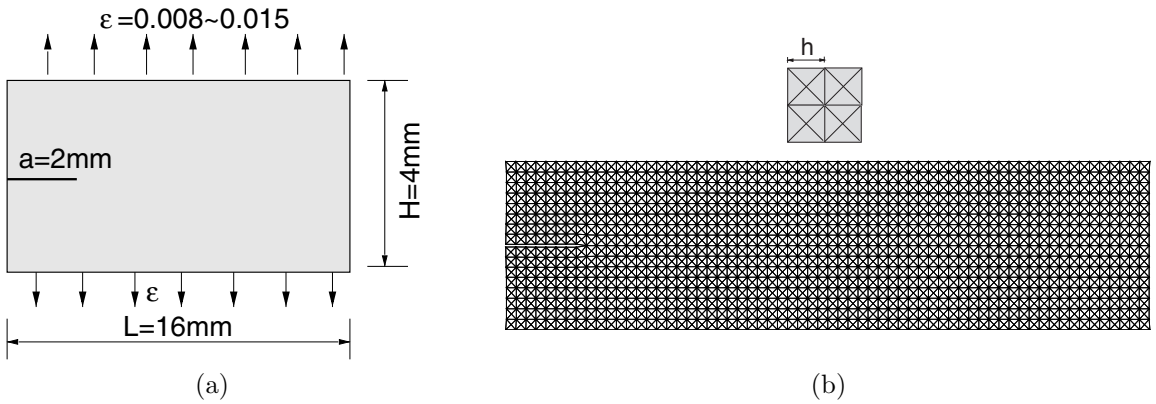

Figure 2: (a) Schematic representation of the geometry and boundary condition for the 2-D steady-state crack propagation problem, using reduced dimension based on Sharon and Fineberg [11]; (b) Mesh discretization of grid 16×64 and characteristic length h=250μm. Other meshes with grid 32×128 (h=125μm), grid 48×192 (h=83μm) and grid 64×256 (h=62.5μm) use the same mesh pattern with different levels of refinement.

Table 1: Properties of PMMA [14] strip subjected to initial stretch.

E (GPa)	ν	ρ (kg/m^3)	G_{Ic} (N/m)	$T_n^{\max} = T_t^{\max}$ (MPa)	$\delta_n = \delta_t$ (μm)	η	c_R (m/s)
3.24	0.35	1190	352.3	129.6	5.44	1	939

In the experiment, the initial load results in an amount of stored strain energy per unit length of approximately $800 - 5000 Nm/m^2$ [11], and a stretch of approximately $\varepsilon = 0.0027$ to 0.0049 along the vertical direction at initial time. To maintain the same energy stored per unit length in the numerical analysis as in the experiment, the stress and strain applied at the initial time are much higher in the former case (numerics) than the latter (experiments). The applied load in the experiment (10 to $18MPa$) is much lower than material tensile strength ($62.1MPa$), while in numerical analyses the initial uniform stress (37 to $96MPa$) is close or even higher than material tensile strength. Therefore, to avoid unwanted fracture at locations without stress concentration, the cohesive strength used in the present study (E/25=$129.6MPa$) is chosen to be higher than the boundary loading. This value does not match the real material tensile strength ($62.1MPa$), and the difference between the actual and reduced dimension must be considered in interpreting the numerical results.

The domain is uniformly discretized by T6 elements of various element sizes as typically shown in Figure 2 (b). Time step Δt is chosen as a fraction (around 10%) of that required by the Courant condition for explicit updating

scheme, to ensure stable computation when cohesive elements are present. Cohesive elements are adaptively inserted in the finite element mesh, which allow crack to spontaneously grow and branch.

5.2 Numerical Results for Various Loading Cases

Driven by the strain energy stored in the pre-stretched strip, the crack propagates towards right edge of the strip. In actual experiments, unless the crack path is constrained, the crack tip speed can hardly reach 50% of Rayleigh wave speed due to energy dissipation mechanisms, for example, from micro crack formation at the immediate crack tip vicinity. The energy dissipation mechanism is simulated by the formation of microbranching at crack tip.

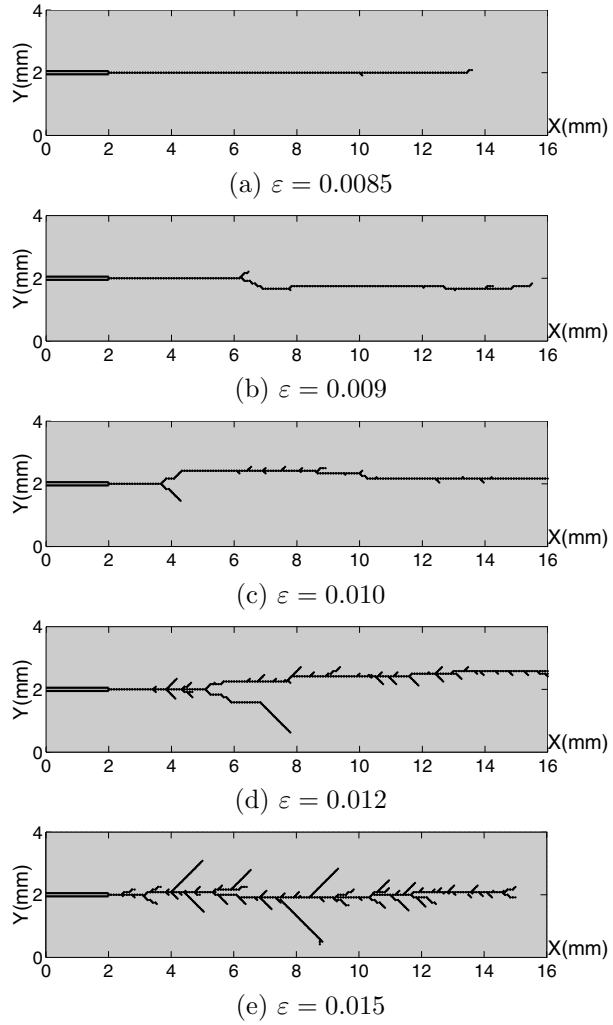

(a) $\varepsilon = 0.0085$

(b) $\varepsilon = 0.009$

(c) $\varepsilon = 0.010$

(d) $\varepsilon = 0.012$

(e) $\varepsilon = 0.015$

Figure 3: Comparison of branch patterns for various loading cases considering different applied strains (ε) and using an initial mesh discretization consisting of a 48×192 grid. (a) $\varepsilon = 0.0085$; (b) $\varepsilon = 0.009$; (c) $\varepsilon = 0.010$; (d) $\varepsilon = 0.012$; (e) $\varepsilon = 0.015$.

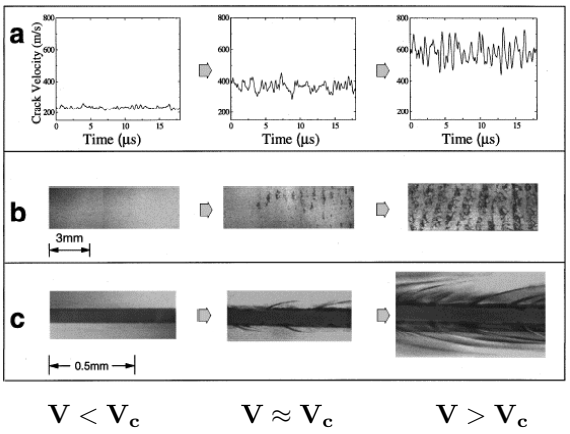

Figure 4: Experimental observation of branching instability as crack propagates in PMMA. Figure reproduced from Figure 4 of Sharon and Fineberg [11]. The critical crack speed at which microbranch appears is denoted as V_c. (**a**) the velocity of the crack transits from smooth function of time at low velocity (left) to oscillatory function at high velocity (right); (**b**) fracture surface transits from smooth surface (left) to coarse texture (right); (**c**) A single crack is observed (left), while microbranches appear at $V \approx V_c$ (center), and increase in length at higher velocities (right).

Experiments [11] indicate that with increasingly stored energy, the crack runs at higher velocity and generates longer and more noticeable microbranches. Figure 3 demonstrates the transition from smooth crack to more roughened crack with significant microbranches as initial stretch increases. The branches plotted in the figure

consist of all the completely separated cohesive surfaces. The condition for cohesive element failure is defined such that all three Gauss points of the elements have experienced complete decohesion (in terms of separation Δ_{eff}). Therefore, some cohesive surfaces that are still active (*i.e.* not all Gauss points have reported decohesion), are not included. Consequently, a "smooth" crack in the plot does not indicate non-existence of any microbranch, rather, it means that even though microbranch may occur, they arrest before running more than one element length.

Table 2: Comparison of crack initiation time and average crack speed for different loading cases as shown in Figure 3.

Initial stretch ε	Mesh grids	Crack initiation time (μs)	Average crack velocity (m/s)
0.0085	48×192	1.61	518
0.009	48×192	1.23	558
0.010	48×192	0.98	572
0.012	48×192	0.71	597
0.015	48×192	0.47	642

Figure 3 indicates that for $\varepsilon = 0.0085$ case, the main crack runs smoothly through the entire strip, while more microbranches appear for $\varepsilon = 0.009$ and $\varepsilon = 0.01$ cases (Figure 3 (b) and (c), respectively). As applied loading increases, the microbranches also extend longer, as shown in Figure 3(d). This overall trends are in agreement with the experiments by Sharon and Fineberg [11] (Figure 4). The crack initiation time and average crack velocity for these loading cases are reported in Table 2. Apparently, crack initiates earlier and runs faster at higher loading.

Other investigations which are conducted but not reported in the current paper include mesh convergence, influence of applied load on crack velocity, as well as energy balance study.

6 CONCLUSIONS

In this study, the dynamic microbranching in brittle materials is investigated. A research code is developed using *explicit* dynamic scheme and employing extrinsic cohesive zone element to model fracture behavior at the crack tip. This finite element framework is supported by a newly proposed [3] adjacency-based topological data structure (TopS), which provides efficient access to the geometrical and topological information necessary for the adaptive insertion of extrinsic cohesive element.

Extrinsic CZM is employed in the investigation, which eliminates the unwelcome artificial compliance associated with intrinsic CZM. The extrinsic model poses challenge both at the implementation stage and at the interpretation of simulation results. The numerical framework is carefully designed to interact with the data structure (TopS) so as to provide robust insertion of cohesive elements.

Numerical simulation is carried out based on a reduced dimension model of a dynamic fracture experiment on PMMA. The numerical results reveal increased roughness of fracture surface, longer microbranches and higher crack speed for increased energy input, which is in accordance with those observed in the experiment. Various numerical issues are discussed in detail, including mesh convergence, cohesive element insertion check time intervals, as well as energy evolution. Apparently, the extrinsic model is successful in reproducing the numerous crack microbranching occurrence. Compared to Miller et al.'s work [4], which employs a potential-based intrinsic CZM for the same problem, the present approach produces simulation results that resemble the experiment better in both the microbranch angle and propagation length. This study thus reveal the importance of adopting extrinsic CZM approach when cohesive elements are inserted extensively in a large region.

REFERENCES

[1] Cox, B.N., Gao, H., Gross, D., Rittel, D., 2005 Modern topics and challenges in dynamic fracture. *Journal of the Mechanics and Physics of Solids* **53**, 565-596.

[2] Celes, W., Paulino, G.H., Espinha, R. 2005. Efficient handling of implicit entities in reduced mesh representations. *Journal of Computing and Information Science in Engineering* **5**, 348-359.

[3] Celes, W., Paulino, G.H., Espinha, R. 2005. A compact adjacency-based topological data structure for finite element mesh representation. *International Journal for Numerical Methods in Engineering* **64**, 1529-1556.

[4] Miller, O, Fruend L. B., Needleman, A. 1999. Energy dissipation in dynamic fracture of brittle materials, *Modelling and Simulation in Materials Science and Engineering* **7**, 573-586.

[5] Ortiz, M., Pandolfi, A., 1999. Finite-deformation irreversible cohesive elements for three-dimensional crack-propagation analysis. *International Journal for Numerical Methods in Engineering* **44**, 1267-1282.

[6] Ravi-Chandar, K. and Knauss, W. G. 1984. An experimental investigation into dynamic fracture-I. Crack initiation and crack arrest. *International Journal of Fracture* **25**, 247-262.

[7] Ravi-Chandar, K. and Knauss, W. G. 1984. An experimental investigation into dynamic fracture-II. Microstructural aspects. *International Journal of Fracture* **26**, 65-80.

[8] Ravi-Chandar, K. and Knauss, W. G. 1984. An experimental investigation into dynamic fracture-III. On steady-state crack propagation and crack branching. *International Journal of Fracture* **26**, 141-154.

[9] Ravi-Chandar, K. and Knauss, W. G. 1984. An experimental investigation into dynamic fracture-IV. On the interaction of stress waves with propagating cracks. *International Journal of Fracture* **26**, 189-200.

[10] Ravi-Chandar, K. and Yang, B. 1997. On the role of microcracks in the dynamic fracture of brittle materials. *Journal of the Mechanics and Physics of Solids*, **45**, 535-563.

[11] Sharon, E. and Fineberg, J. 1996. Microbranching instability and the dynamic fracture of brittle materials. *Physical Reviews B* **54**, 7128-7139.

[12] Sharon, E., Gross, S. P. and Fineberg, J. 1995. Local crack branching as a mechanism for instability in dynamic fracture. *Physical Review Letters* **74**, 5096-5099.

[13] Sharon, E., Gross, S. P. and Fineberg, J. 1995. Energy dissipation in dynamic fracture. *Physical Review Letters* **76**, 2117-2120.

[14] Xu, X. and Needleman, A. 1995. Numerical simulations of dynamic crack growth along an interface, *International Journal of Fracture* **74**, 289-324.

[15] Zhang, Z. and Paulino, G. H. 2005. Cohesive zone modeling of dynamic failure in homogeneous and functionally graded materials, *International Journal of Plasticity* **21**, 1195-1254.